Earth and Planetary Science Letters 453 (2016) 252–259

Contents lists available at ScienceDirect

Earth and Planetary Science Letters

www.elsevier.com/locate/epsl

Balloon-borne measurement of the aerosol size distribution from an Icelandic flood basalt eruption

D. Vignelles [a,*], T.J. Roberts [a], E. Carboni [b], E. Ilyinskaya [c], M. Pfeffer [d], P. Dagsson Waldhauserova [e,f,g], A. Schmidt [c], G. Berthet [a], F. Jegou [a], J.-B. Renard [a], H. Ólafsson [h], B. Bergsson [d], R. Yeo [d], N. Fannar Reynisson [d], R.G. Grainger [b], B. Galle [i], V. Conde [i], S. Arellano [i], T. Lurton [a], B. Coute [a], Vincent Duverger [a]

[a] LPC2E/CNRS, Université d'Orléans, 3A, Avenue de la Recherche Scientifique, 45071 Orléans, France
[b] COMET, Atmospheric, Oceanic and Planetary Physics, University of Oxford, Parks Road, Oxford, OX1 3PU, UK
[c] School of Earth and Environment, University of Leeds, LS2 9JT, Leeds, UK
[d] Icelandic Meteorological Office, Bústaðavegi 7–9, 150 Reykjavik, Iceland
[e] University of Iceland, Departments of Physical and Earth Sciences, Reykjavik, Iceland
[f] Agricultural University of Iceland, Faculty of Environment, Hvanneyri, Iceland
[g] Czech University of Life Sciences Prague, Prague, Czech Republic
[h] University of Iceland, Icelandic Meteorological Office and Institute for Meteorological Research, Reykjavík, Iceland
[i] Chalmers University of Technology, Department of Earth and Space Sciences, Hörsalsvägen 11, 412 96 Gothenburg, Sweden

ARTICLE INFO

Article history:
Received 28 January 2016
Received in revised form 11 August 2016
Accepted 17 August 2016
Available online 31 August 2016
Editor: B. Marty

Keywords:
volcano plume
balloon
in-situ measurement
aerosol counter
Iceland

ABSTRACT

We present in situ balloon-borne measurements of aerosols in a volcanic plume made during the Holuhraun eruption (Iceland) in January 2015. The balloon flight intercepted a young plume at 8 km distance downwind from the crater, where the plume is ~15 min of age. The balloon carried a novel miniature optical particle counter LOAC (Light Optical Aerosol Counter) which measures particle number concentration and size distribution in the plume, alongside a meteorological payload. We discuss the possibility of calculating particle flux by combining LOAC data with measurements of sulfur dioxide flux by ground-based UV spectrometer (DOAS).

The balloon passed through the plume at altitude range of 2.0–3.1 km above sea level (a.s.l.). The plume top height was determined as 2.7–3.1 km a.s.l., which is in good agreement with data from Infrared Atmospheric Sounding Interferometer (IASI) satellite. Two distinct plume layers were detected, a non-condensed lower layer (300 m thickness) and a condensed upper layer (800 m thickness). The lower layer was characterized by a lognormal size distribution of fine particles (0.2 µm diameter) and a secondary, coarser mode (2.3 µm diameter), with a total particle number concentration of around 100 cm^{-3} in the 0.2–100 µm detection range. The upper layer was dominated by particle centered on 20 µm in diameter as well as containing a finer mode (2 µm diameter). The total particle number concentration in the upper plume layer was an order of magnitude higher than in the lower layer.

We demonstrate that intercepting a volcanic plume with a meteorological balloon carrying LOAC is an efficient method to characterize volcanic aerosol properties. During future volcanic eruptions, balloon-borne measurements could be carried out easily and rapidly over a large spatial area in order to better characterize the evolution of the particle size distribution and particle number concentrations in a volcanic plume.

1. Introduction

Volcanoes release gases and particles into the atmosphere through continuous degassing or episodic eruptive events, and depending on the injection altitude and emission rate, they can impact both the tropospheric and stratospheric composition and climate (McCormick et al., 1995; Robock, 2000; Schmidt et al., 2012; Solomon et al., 2011). Ash-rich plumes such as that from the Icelandic Eyjafjallajökull eruption in 2010 can lead to widespread disruption of aviation (Spinetti et al., 2013). Ash-poor volcanic plumes may also strongly impact the environment and quality of life due to high concentrations of polluting gases and aerosol

* Corresponding author.
E-mail address: damien.vignelles@cnrs-orleans.fr (D. Vignelles).

http://dx.doi.org/10.1016/j.epsl.2016.08.027
0012-821X/

particles. Indeed, the recent flood basalt eruption at Holuhraun (31 August 2014–27 February 2015, 1.6 km^3 of erupted lava, Gislason et al., 2015) was a major source of sulfur gases and aerosols and caused both local (Gislason et al., 2015) and European-wide (Schmidt et al., 2015) deteriorations to air quality.

Long-lasting flood basalt eruptions are one of the most hazardous volcanic scenarios in Iceland and have had enormous societal and economic consequences across the northern hemisphere (Gudmundsson et al., 2008). One of the best known examples is the Laki eruption (1783-84 CE) (Thordarson and Self, 2003) which led to deaths of >20% of the Icelandic population by environmental pollution and famine, and likely increased European levels of mortality through air pollution by sulfur-bearing gas and aerosol (Grattan, 1998; Taylor et al., 2003; Witham and Oppenheimer, 2004). Potential impacts of such an eruption on modern day Europe have been modeled by Schmidt et al. (2011) who found that PM2.5 aerosol pollution would double causing 142,000 additional cardiopulmonary fatalities in the year following the eruption onset. A Laki-type eruption scenario has been recently included in the UK National Risk Register (UK Cabinet Office, 2013). However, there are still many uncertainties about the source terms of Icelandic flood basalt eruptions that are necessary for atmospheric models and health impact assessments. The 2014–2015 Holuhraun eruption was therefore a unique opportunity to study the near-source composition of an Icelandic flood basalt eruption plume.

Direct measurements of volcanic aerosol (defined here as non-silicate particles such as sulfate) are needed to better constrain the plume sulfur chemistry and particle processes, which together with plume injection height are two key uncertainties in models used to predict the dispersion and air quality impacts from eruptions. Existing in-situ measurements of elevated volcanic plumes mostly involve interception of aged plumes that have already undergone significant chemical and physical evolutions (Marenco et al., 2011; Jégou et al., 2013). Small portable sensors placed on airborne drones or balloons offer new possibilities to characterize volcanic plumes close to source. McGonigle et al. (2008) demonstrated heli-type drone sensing of SO_2 and CO_2 to determine CO_2 fluxes at Vulcano fumarole field (Italy). More recently, Shinohara (2013) deployed a suite of gas sensors on a drone to characterize the plume of Kirishima volcano (Japan) during an eruptive phase where ground-based sampling was too hazardous. Pieri et al. (2013) performed drone as well as balloon-based campaigns to measure gases and ash particles in the eruptive plume of Turrialba volcano (Costa Rica).

Here we present measurements made by a newly developed lightweight optical aerosol counter (LOAC) carried on a meteorological balloon through the near-source Holuhraun eruption plume. By combining size-resolved particle number concentration measurements with meteorological parameters and remote sensing of SO_2 flux, we are able to provide some of the key eruption source term information.

2. Holuhraun and plume conditions

Holuhraun is located northwards of the Vatnajökull ice cap in the largest desert area of Iceland. On January 22nd 2015, visible plumes were emitted from the main crater (Baugur) and several places within the lava field (Fig. 1). It was estimated that ~90% of the released gas volume was from Baugur. These distinct plumes merged into one main plume which was advected northeastwards. The rising plume visibly changed while being advected, with the upper part turning into a condensed, optically thick cloud several kilometers downwind of the source. The atmosphere was very clear within the boundary layer, and the lower troposphere was cloud-free except for the volcanic plume. Clouds were visible at a much higher altitude (>5.5 km above the sea level (a.s.l.) as described in Section 4). Fig. 1 shows the conditions at the eruption site on January 22nd at 14 UTC. The visual appearance of the plume remained consistent throughout the day. Plume dispersion modeling (Iceland Met Office, CALPUFF model, Barsotti et al., 2008) predicted that the northeastward plume advection continued during the night of January 22nd when our balloon-borne measurements were made (see online Appendix 1 for further details). Although the CALPUFF model predicts only ground-level plume exposure, the constant vertical wind profile calculated by HARMONIE model for Holuhraun area (see Section 4) allows us to assume a consistent plume transport direction from ground level up to 4 km a.s.l.

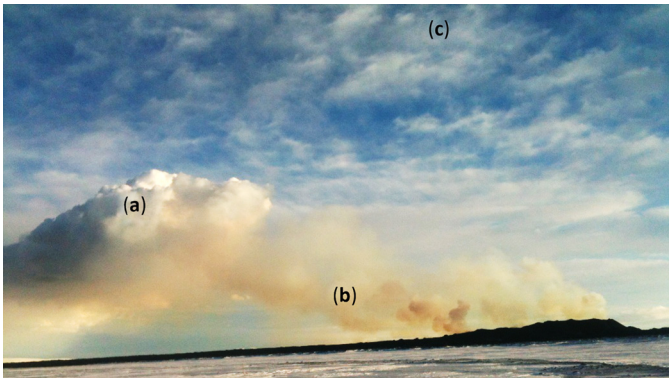

Fig. 1. Picture taken at 14 UTC on January 22nd 2015 during the afternoon before the balloon flight. a) Condensed plume, b) non-condensed plume, c) high altitude clouds.

3. Methods

3.1. Balloon instrumentation

The LOAC (Light Optical Aerosol Counter) is an optical particle counter sufficiently lightweight to be carried by a 1000 g meteorological balloon. The instrument contains a laser (650 nm) and measures the intensity of light scattered at two angles, 12° and 60° (Lurton et al., 2014; Renard et al., 2016) to discriminate the particle concentration over 19 size classes from 0.2 µm to 100 µm in diameter. Sampling is driven by a miniature pump (constant flowrate of 2 $L\,min^{-1}$) enclosed in the gondola with the air pumped through the measurement cell and released afterwards. For the LOAC integration time of 10 s, the counting uncertainty is derived from the Poisson counting statistics and defined as one relative standard deviation: 60% for a particle number concentration of 10^{-2} cm^{-3}, 20% for 10^{-1} cm^{-3} and 6% for a particle number concentrations higher than 1 cm^{-3}. A complete description of the instrument can be found in Renard et al. (2016). Differences in scattering between the two distinct angles are also used to determine the typology. The typology is a specific term related to the main refractive index of particles sampled, obtained by combining the intensities of light scattered at two diffusion angles (Renard et al., 2016). This can provide information on the nature of the particles, determined by reference to laboratory measurements (Renard et al., 2016). The typology gives several classes of optical properties discussed in Section 5.3. The aerosol data, GPS coordinates, temperature and hygrometry are sent in real time by a telemetry system. The flight chain configuration is shown in Fig. 2.

To aid interpretation, the balloon data are analyzed in conjunction with model outputs (backward trajectories, air quality plume dispersion and meteorological model) and remote sensing data (ground-based DOAS, and satellite Infrared Atmospheric Sounding Interferometer (IASI) overpasses) in the Results Section 4.

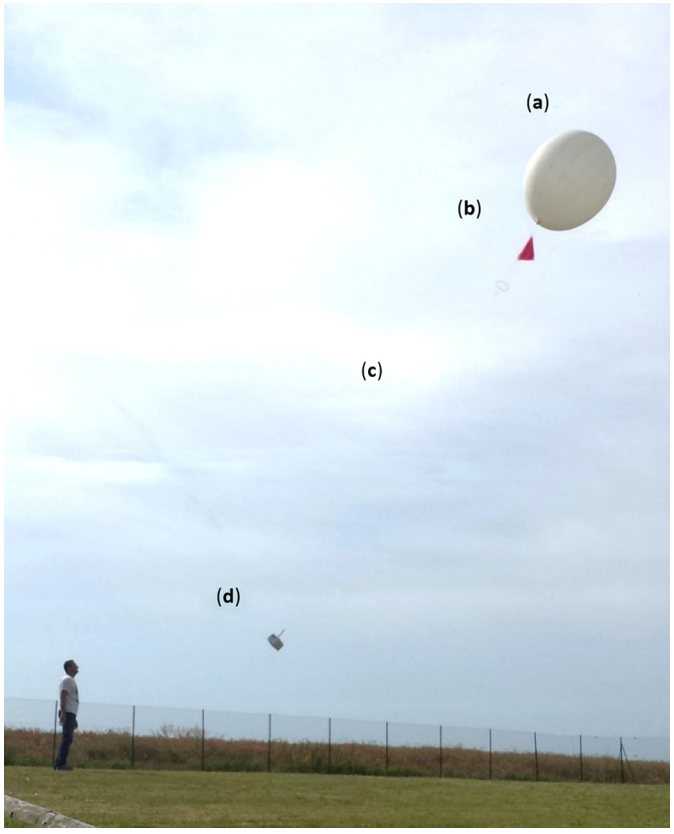

Fig. 2. Typical flight configuration of a LOAC under a weather balloon. We use a 1000 g latex balloon (a), a parachute (b), 10 m aeronautical flight chain (c) and a gondola (d). The gondola includes a LOAC and a MeteoModem telemetry system which measures the air temperature and the hygrometry. Data are sent to the ground station by telemetry and are not stored in the gondola.

3.2. Balloon flight

The balloon launch represented a considerable challenge due to a combination of very difficult conditions. The meteorological balloon and payload instrumentation were prepared on site on January 22nd after nightfall. The balloon was inflated during the hours of darkness, with ambient air temperature $<0\,^{\circ}\mathrm{C}$ and a relatively high wind speed of $\sim 10\ \mu\mathrm{m\,s}^{-1}$. The ground telemetry station was powered by car batteries due to the remoteness of the launch site.

The balloon borne instruments were launched at 64°56′01″N, −16°40′39″E at 21 UTC on January 22nd 2015, 9 km N–NE from the Holuhraun main eruptive crater (64°52′21″N, −16°49′42″E), at 700 m a.s.l. The location of the launch site (directly under the plume) was chosen based on the modeled plume advection direction (CALPUFF, Barsotti et al., 2008, see online Appendix 1). Backward trajectories confirm that the launch site was chosen successfully with regard to air mass movement from the Holuhraun eruptive crater (Fig. 3). The backward trajectories are calculated with FLEXTRA 5.0 code which is a 3D kinetic trajectory calculation code (Stohl et al., 1998). Trajectories are initialized using global 3-hourly ECMWF (European Center for Medium-Range Weather Forecasts) reanalysis data with 1° × 1° horizontal resolution for a period of 24 h from 21 UTC on January 22nd and at every 200 m above the balloon launching position up to 14 km. For clarity, Fig. 3 presents only the backward trajectories initialized at 2.4 km and 4.0 km, corresponding to the height of the plume and the air mass above the plume respectively. All trajectories show the same direction of advection indicating that the wind direction was similar from ground level to altitudes above the top of the plume (plume

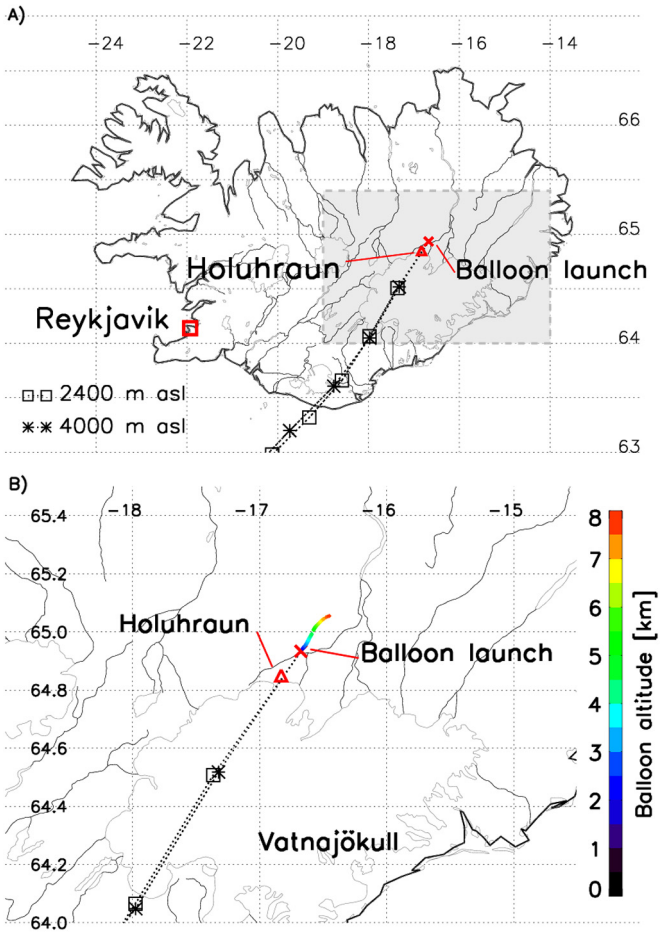

Fig. 3. A) Holuhraun eruption site (main crater) is shown by a red triangle and the balloon launch location by a red cross. Two backward trajectories intercepting the balloon launch position are shown for 2.4 km–4.0 km a.s.l. range. The gray area is shown in close-up on figure B). B) also shows the balloon flight path as a function of altitude, where altitude is represented by a color scale. (For interpretation of the references to color in this figure legend, the reader is referred to the web version of this article.)

top determined by aerosol observations, see Section 5.1). Based on the FLEXTRA backward trajectories, we were also able to determine the average age of the plume when the balloon crossed it, considering only a horizontal advection and constant velocity of the air mass between the two final hours of the trajectories. This calculation gives an air mass age of 10–15 min.

Data were recorded during the ascent and transmitted by telemetry. The meteorological parameters were recorded with a frequency of 1 Hz. The particle concentration is measured by the LOAC aerosol counter every 10 s, and the typology based on the aerosol optical properties is obtained every 60 s. Due to a technical problem with the telemetry system, particle concentration data was not obtained from ground level up to ∼1.7 km a.s.l. Data were recorded from 1.7 km up to 8 km a.s.l. with a small number of data points lost during telemetry, mostly in the altitude range between 4.4 km and 4.8 km a.s.l.

4. Results

Fig. 4 shows the total number concentration of particles (TPC) sized between 0.2 µm and 100 µm in diameter, the vertical velocity of the balloon and the relative humidity (RH) as a function of altitude (see online Appendix 2 for size distributions as a function of altitude). On each plot we have determined 6 altitude-dependent Zones with different characteristics (Fig. 4). The 6 distinct Zones

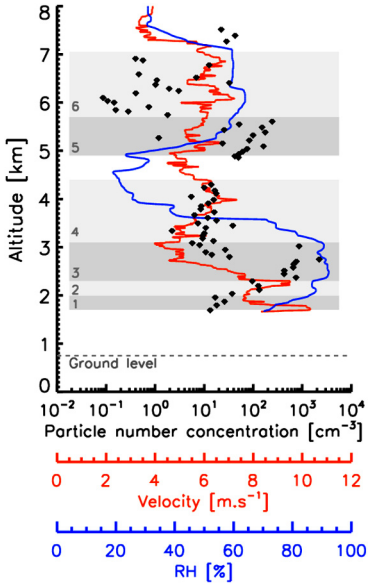

Fig. 4. Flight parameters measured during the balloon ascent. Particle number concentration (size range 0.2–100 µm diameter) as black dots; balloon vertical velocity as orange line; relative humidity as blue + line. The six gray rectangles are referring to the six Zones determined by the vertical evolution of the flight parameters. (For interpretation of the references to color in this figure legend, the reader is referred to the web version of this article.)

were determined based on the correlation between RH and particle number concentration profile. Fig. 5 shows the optical typology detected by the LOAC in different size bins. Most notable are two distinct Zones of liquid droplets (∼2.5–3 km a.s.l., Zone 3) and ice particles (around ∼6–7 km a.s.l., Zone 6) which correspond to distinct water/ice cloud layers. Further discussion of the particle size distribution and its typology across the identified Zones is in Section 5.

Zone 1 (1.7–2.0 km a.s.l.) presents a high and structured vertical velocity profile, an increasing RH with altitude and a relatively low number concentration of particles (∼5 cm^{-3} in 0.2 µm to 100 µm detection range). This Zone is representative of the atmosphere underneath the volcanic plume.

Zone 2 (2.0–2.3 km a.s.l.) is characterized by a higher RH and higher particle concentration than Zone 1 (∼100 cm^{-3}). The particle size distribution shows two size modes and the typology indicates a distinct absorbing particle nature. Zone 2 is the plume in a non-condensed phase.

Zone 3 (2.3–3.1 km a.s.l.) has particle concentration greater than 500 cm^{-3}, and the typology indicates liquid droplets. Zone 3 is the plume in the condensed phase. This assumption is validated by the rapidly decreasing vertical velocity measured above 2.3 km a.s.l. which indicates a change in the air mass composition. Liquid droplets are condensing onto the balloon, increasing its mass and causing the vertical velocity to decrease from 10 $m\,s^{-1}$ to 4 $m\,s^{-1}$. This deduction is also consistent with the hygrometry measurements that indicate a high RH above 2.3 km a.s.l. Zone 3 is discussed further in Section 5.2. The upper part of Zone 3 is placed at 3.1 km a.s.l. even though the particle concentration in 2.8 km to 3.0 km a.s.l. is close to the background level in Zone 1. We assume dynamical processes can locally modulate the particle concentration profile (plume layering). The altitude of the top of the plume (2.8–3.1 km a.s.l.) represents a very precise placement and is in good agreement with an estimate from satellite data as discussed further in Section 5.1 (Fig. 6).

To further determine if Zone 3 is a condensed plume or a non-volcanic meteorological cloud, we have used a non-hygrostatic convection-permitting model developed by Météo-France and AL-

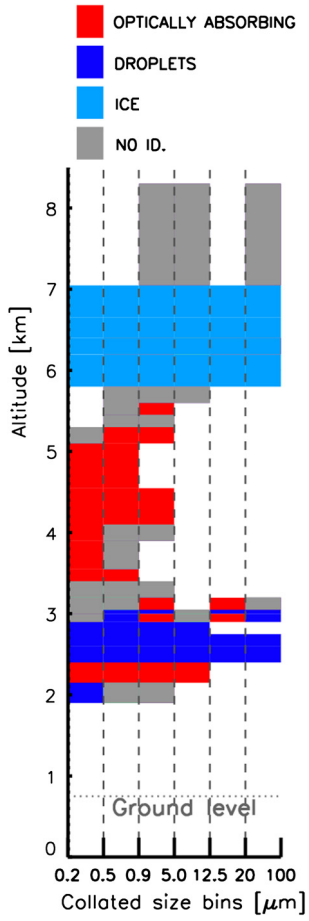

Fig. 5. The dominant optical nature (typology) for 6 collated size bins as a function of altitude. The different colors represent the bulk nature of the aerosol.

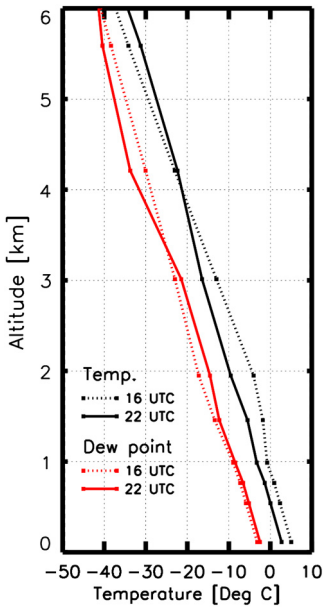

Fig. 6. Outputs from the HARMONIE model for the Holuhraun region (2.5 km^2). It shows the column profile for temperature (black) and dew point (red) over the eruption site at 16 UTC (dashed lines) and 22 UTC (unbroken lines). The balloon was launched at 22 UTC. Cloud formation is expected when the temperature and the dew point match. The model does not predict cloud formation at either 16 UTC or 22 UTC. (For interpretation of the references to color in this figure legend, the reader is referred to the web version of this article.)

ADIN based on the AROME model from Météo-France (Seity et al., 2011, Brousseau et al. 2011) named HARMONIE. Firstly, outputs from the HARMONIE model for both 16 UTC and 22 UTC focused on the Holuhraun region confirm that the meteorological situation was very similar between daytime (Fig. 1) and nighttime when the balloon was launched, i.e. that there were no meteorological clouds at this altitude. Fig. 5 presents the temperature and the dew point for both daytime and nighttime scenarios, showing very similar profiles in temperature and maximum dew point. Secondly, the output from HARMONIE does not indicate any low-level cloud, because the temperature is higher than the dew point over the plume altitude range. This model is not sensitive to the Holuhraun eruption plume and therefore presents the meteorological conditions without the contribution of the volcanic plume.

Zone 4 (3.1–4.4 km a.s.l.) is air mass overlying the volcanic plume. A low total particle number concentration was found in this Zone, ~5–10 cm^{-3} in the 0.2 µm to 100 µm detection range. This Zone represents the background conditions and the TPC is found near constant with increasing altitude. However, RH is higher between 3.1 km and 3.6 km a.s.l. which may be an instrument effect caused by persistence of humidity on the sensor. The particle number concentration and size distribution in Zone 4 is similar to that of Zone 1. Our interpretation is that the boundaries between Zones 1 and 2, and 3 and 4 determine the bottom and top boundaries of the volcanic plume, respectively.

Zones 5 and 6 (respectively 4.9–5.7 km a.s.l. and 5.7–7.1 km a.s.l.) are discussed here only briefly in order to show the complete profile of the flight. Between 4.4 km and 4.9 km a.s.l. we lost the signal from the gondola. Zone 5 is assumed to be a background air mass influenced by the icy cloud determined in Zone 6. The typology clearly identifies Zone 6 particles to be an icy cloud corresponding to the high altitude clouds visible on Fig. 1.

5. Discussion

5.1. Plume Height

We compare our plume height observation (2.0–3.1 km a.s.l., with a condensed layer at 2.3–3.1 km a.s.l.) to an independent estimate of the plume height from IASI data on Meteorological Operational (MetOp) Satellite. This novel technique of retrieving plume height from satellite data is described by Carboni et al. (2012) and has been applied to several volcanic eruptions (Carboni et al., 2016). Here we report only a summary of the algorithm. The optimal estimation technique of Rodgers (2000) is employed to estimate the SO_2 plume, and the surface skin temperature using simultaneously all IASI measurements from 1000 to 1200 cm^{-1} and from 1300 and 1410 cm^{-1} (the v_1 and the v_3 SO_2 bands). The retrieval is effected by minimizing a cost function J defined as (E1).

$$J = \left(y - F(x)\right)^T S_y^{-1}\left(y - F(x)\right)^{-1} + (x - x_a)^T S_a^{-1}(x - x_a)^{-1} \quad \text{(E1)}$$

Where $F(x)$ is the forward model (i.e. the function which maps the state parameters to measurements), x is the vector of retrieved values, y the measurement vector, S_y is the measurement error covariance matrix, x_a is the a priori error covariance matrix. The forward model is based on a radiative transfer code (RTTOV) (Saunders et al., 1999) extended to include SO_2 explicitly, and uses ECMWF temperatures interpolated to the measurement time and location. Note that the SO_2 IASI retrieval is not affected by underlying cloud, and rigorous error propagation – including the incorporation of forward model and forward model parameter error – is built into the system, providing quality control and error estimates on the retrieved state for every pixel. The presence of water droplets is included in the error estimate of the retrieval scheme

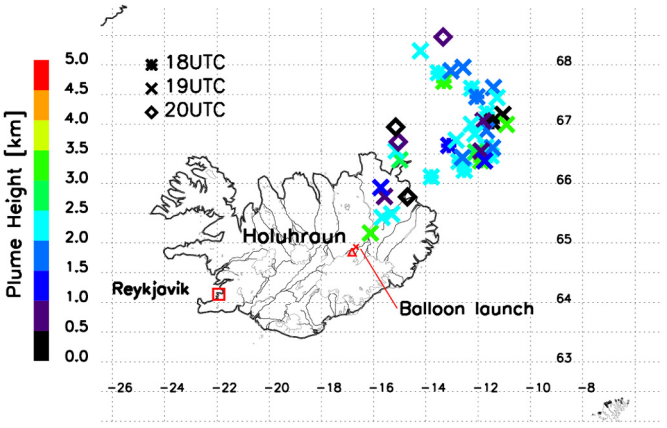

Fig. 7. Plume height for three overpasses of MetOp satellite at 18, 19 and 20 UTC on January 22nd from IASI retrieval method (Carboni et al., 2012). Each measurement is represented by a symbol and a color. Each symbol represents the time of the satellite overpass (star: 18 UTC, cross: 19 UTC, diamond: 20 UTC). Colors represent the retrieved plume altitude. (For interpretation of the references to color in this figure, the reader is referred to the web version of this article.)

(spectra with water droplets are used to compute the error covariance matrix see Carboni et al. (2012) and should not affect the retrieval). This is confirmed by the comparison of altitude of the SO_2 plume from the IASI scheme and CALIPSO backscatter profile in Carboni et al. (2016).

Fig. 7 shows the contribution of three overpasses of MetOp over Iceland on January 22nd at 18, 19 and 20 UTC (within hours of our balloon flight). The altitude given by the Carboni algorithm of the closest measurement from the crater is 3.0 ± 1.1 km a.s.l. This altitude is consistent with the altitude detected by the LOAC which determines the top height of the plume in the 2.7–3.1 km a.s.l. range, even though the two estimates are based on data collected 30 km apart. Thus the LOAC balloon flight is an in-situ validation of the recently developed Carboni et al. (2012) method for plume altitude estimation by IASI satellite retrieval. Altitude estimation of volcanic plumes is critical for modeling plume advection, chemical processing and atmospheric impacts, and can be a key uncertainty in the estimation of SO_2 burdens from satellite.

5.2. Particle size distribution in the plume

The particle size distribution in Zones 1–4 (number and volume distributions) have been fitted using a lognormal distribution modes described by equation (E2). Shape parameters for each distribution are shown in Table 1 (see Fig. A3 for details in online Appendix 3).

$$V(d) = \frac{V_0}{\sigma_N \sqrt{2\pi}} e^{\left(-\frac{1}{2}\left(\frac{\log(d) - \mu_v}{\sigma_N}\right)^2\right)} \quad \text{(E2)}$$

Where $V(d)$ is the volume density distribution with shape parameters: σ_N and μ_v and the amplitude parameter V_0 were determined by least-squares fitting to the LOAC observations.

Firstly, we observe that the size and volume distributions for Zones 1 and 4 (both identified as background air, outside of the volcanic plume) are of similar proportions, with similar median diameter (μ_v) and standard deviation (σ_N). We assume that this mono-modal background particle distribution is also a representative background for Zones 2 and 3 where the plume is present. Clear bimodal particle distributions are observed in Zones 2 and 3, which dominate over the background signature. The bimodal distribution consists of sub-micron and supra-micron modes in Zone 2, attributed to non-condensed plume. In the condensed plume of Zone 3 both of the dominant modes are supra-micron.

Table 1
Parameters from the log-normal fitting of volume concentration measured by the LOAC for the first four Zones. Zone 1 and Zone 4 represent background (non-volcanic) air mass. The volcanic plume is present in Zones 2 and 3.

	Zone 1	Zone 2		Zone 3		Zone 4
	Background	*Non-condensed plume*		*Condensed plume*		*Background*
		Mode 1	Mode 2	Mode 1	Mode 2	
Median diameter [μm]	0.1	0.2	2.3	2.1	19.6	0.1
Standard deviation [μm]	2.3	2.3	2.0	2.4	1.9	2.0
Total volume [μm^3]	1.2	3.6	2.0	79.1	$9.8 \cdot 10^4$	0.4

More precisely, Zone 2 presents a size distribution that is higher in particle number than Zone 1 for particles <1 μm, with the maximum of the dominant size mode presumably below the detection range (<0.2 μm), and with the secondary mode around 2 μm (all parameters summarized in Table 1).

The condensed plume in the Zone 3 has a dominant size mode ∼2.1 μm, greater than Zone 2 (∼0.2 μm), and a secondary mode with diameter of 19 μm. Such particle modes around 10 μm are characteristic for clouds (Warner, 1969; Hammer et al., 2014). Typology clearly shows the presence of liquid droplets. Water cloud droplet formation is expected based on the presence of submicron particles both in the background air and the plume, which can act as cloud condensation nuclei, facilitated by the H_2O-richness of the volcanic plume. The measured vertical concentration profile in Zone 3 may be affected by "shadowing effect" an instrumental effect that can lead to underestimation of the number of fine particles when larger particles are simultaneously present in the measurement cell (Renard et al., 2016). In addition, a reduced number of small particles in the presence of larger particles might indicate that fine particles grow by condensation or coagulation processes. The phenomenon is apparent between 2.4 and 2.7 km a.s.l. where large particles appear in the first layer of the condensed plume (Fig. 4). This part of Zone 3 is flanked by two layers with fewer large particles and >10 times greater concentration of smaller particles compared to the inner region where a relatively greater number of large particles is detected. It is also indicative of plume heterogeneity.

The air masses above the volcanic plume (Zones 4 and 5) have a relatively constant particle size distribution, close to the size distribution in Zone 1. The typology shows a high complex refractive index related to absorbing particles. Between 5.5 and 7.0 km a.s.l. an icy cloud becomes present (Zone 6). This occurs in a region of higher RH and is highlighted both by both the size-resolved aerosol particle number and the typology, Fig. 5.

5.3. Optical particles index, the "Typology"

In Zone 2 (non-condensed volcanic plume), the typology based onto the optical properties of particles does not reveal a clear optical nature. It gives an optically absorbing signature, however we assume the observed particles to be most likely dominated by water–sulfate mixture, based on particle measurements from non-explosive ash-poor volcanic emissions made elsewhere (e.g. Kroll et al., 2015). Volcano emissions are chemically reactive and the sulfate aerosol can be formed through high-temperature oxidation at near-magmatic temperatures (Ilyinskaya et al., 2012; Martin et al., 2006; Roberts et al., 2014) as well as the slower atmospheric oxidation of emitted SO_2 at ambient temperatures. A possible complication for determining typology from particle scattering can be the presence of internally mixed aerosol, or particles of different kinds in the same sampling period. Nevertheless, the result is that the nature of the particles are different between Zone 1 (background air) and Zone 2 (non-condensed plume).

In Zone 3 the typology gives an unambiguous droplet signature. Here the condensed phase is clearly established. This also confirms the hygroscopic nature of the volcanic particles. Condensed water on the volcanic particles both increases their size (Section 4) and acts to dilute any absorbing component to the extent that the typology yields a droplets signature.

The typology is less well resolved than the particle concentration over the altitude profile but also indicates the same plume layering in the 2.8–3.0 km a.s.l. range where a thin layer of non-condensed plume was found (Section 4).

Typology is similar for Zones 4 and 5. Typology for Zone 6 (ice) is clearly established and different from Zones 4 and 5. It strongly supports the presence of icy clouds at high altitude.

5.4. Particle flux

The Holuhraun eruption emitted at least 3 times more SO_2 per day than all 28 EU states in 2010 (European Environmental Agency (EEA), 2014). Fluxes of SO_2 reached 120 kt/d in September 2014, with a total emission of 2.0 ± 0.6 Tg during that month (Schmidt et al., 2015), and 11 ± 5 Tg of SO_2 for the whole eruption (Gíslason et al., 2015). Nevertheless, particle fluxes have not been estimated for this eruption even though particles play an important role in plume heterogeneous chemistry (Roberts et al., 2014), as well as climate impacts (Schmidt et al., 2012).

Here we provide a particle flux estimate by combining the LOAC observations and remote sensing of SO_2. The particle number concentration was measured at 8 km downwind of the main crater (15 min from emission), therefore the total particle flux calculation will be representative only of this location relative to the emission source and taking into account the specific wind and microphysical conditions.

Within the 300 m thick non-condensed plume (Zone 2) we measured on average ∼100 particles cm^{-3} over the 0.2–100 μm size range. Using this particle number concentration measurement we make a calculation to roughly estimate the particle flux. This flux cannot be calculated directly by combining the particle number concentration and the plume volume because the width of the plume is unconstrained. Instead we propose to determine a ratio between the number of particles and the SO_2 mass concentration in order to estimate the particle flux. Because SO_2 was not co-measured during the LOAC balloon flight, the calculation is only approximate. The SO_2 concentration and flux was measured by a scanning DOAS spectrometer (Galle et al., 2010), located 10 km from the main vent (64°53′3.78″N, −16°40′31.70″E). The DOAS uses scattered sunlight in the UV spectrum to derive path-integrated concentrations (columns) of SO_2. The instrument's viewing direction is rotated along a conical surface from horizon to horizon. When this cone intersects a plume, the total number of molecules of SO_2 in a cross section of the plume can be determined. The flux through the cross section was calculated by NOVAC Program software (Galle et al., 2010) using wind speeds and directions determined by HARMONIE numerical prediction model and a plume height of 2.1 km a.s.l., which is the average triangulated plume height when two DOAS instruments detected the plume. Column SO_2 density of up to 800 DU (time average of 200 DU during the daytime) was detected on the day of the flight,

(one Dobson unit (DU) is equivalent to 2.69×10^{16} molecules cm^{-2} SO_2 column). The average emission rate of SO_2 on January 22nd was calculated as 400 kg/s SO_2 (see online Appendix 4 for SO_2 time series).

The particle to SO_2 ratio is then combined with the flux of SO_2 on the day of the balloon launch to estimate the particle flux. The method is described in the equation (E3) and detailed below.

$$\Phi_{part} = \Phi_{SO_2} \times R \quad \text{where } R = \frac{n_{part}}{m_{SO_2}} \quad \text{and}$$
$$m_{SO_2} = \frac{DU \times m_{mole(SO_2)}}{e} \tag{E3}$$

Φ_{part} is the particle flux in particles per second, Φ_{SO_2} is the SO_2 flux measured in kg of SO_2 per second, R is the ratio between the number of particles and the mass of SO_2 measured in the plume, n_{part} is the number of particles measured in the plume and m_{SO_2} the mass of SO_2. m_{SO_2} is determined with the column density DU in molec.cm^{-2}, the molecular mass $m_{mole(SO_2)}$ in kg $molec^{-1}$ and the plume thickness e in cm.

Assuming 200 DU of SO_2, a particle number concentration of 100 cm^{-3}, and plume thickness of 300 m, we obtain a ratio of 5×10^{12} particles per kg of SO_2. Combining this with the SO_2 flux of 400 kg s^{-1} yields a particle flux of 2×10^{15} per second (particle size range 0.2–100 μm). Our particle flux estimation is highly dependent on our assumption that the plume remained constant during daytime (DOAS measurement) and nighttime (LOAC measurement) on January 22nd. Other sources of uncertainty are the assumed homogeneity of the aerosol within the volcanic plume, the representability of the aerosol profile over an entire plume during several hours, and the fact that our particle/SO_2 ratio calculation combines remote sensing and in-situ observations. However, even if our flux estimation is highly uncertain, we anticipate making future balloon flights in volcanic plumes where LOAC instrument is co-located with SO_2 sensors. This is anticipated to improve accuracy in the calculation of the particle number to SO_2 ratio.

6. Conclusion

This study demonstrated that the newly developed lightweight balloon-borne aerosol counter, LOAC, is an effective method to detect and characterize aerosol properties in volcanic plumes close to the eruptive source. We were able to determine with great accuracy the altitude of the plume top and bottom, identify and characterize distinct layers in the plume as a result of different hygroscopic phases of the plume based on the measured particle size distribution.

Volcanic plumes are known to impact cloud formation and cloud microphysical properties through volcanic aerosol acting as cloud condensation nuclei (Martucci et al., 2012; Schmidt et al., 2012, and Spiridonov et al., 2013). In the case of Holuhraun, the cloud observed on January 22nd 2015 near the eruption site was mainly formed due to the presence of hygroscopic volcanic particles and excess water vapor in the near-source plume. Volcanic emissions are typically dominated by H_2O. Gaseous H_2O is quickly condensed after emission into the cold atmosphere. Such cloud formation may facilitate processes (e.g. aqueous-phase oxidation of SO_2) that could alter the plume properties and downwind impacts.

We have tested a new launch-on-command capacity for combined volcano particle and plume height characterization during an effusive volcanic eruption that could be applied not only near the volcanic source as demonstrated in this study but also to the more dilute plume further downwind. Meteorological balloons with LOAC instrument payloads can be launched by non-specialist personnel and are low-cost compared to other methods such as aircraft measurements. This method can also potentially be used to characterize the evolution of the particle size distribution and particle number concentrations in volcanic plumes of a large-magnitude explosive eruption that injects sulfur into the stratosphere. Several LOAC balloon payloads are currently being kept ready for launch in Iceland and France as well as several volcanoes elsewhere (e.g. the Île de la Réunion, Indian Ocean).

Our measurements of the near-source Holuhraun plume provide a valuable dataset for the initialization of plume dispersion models which can assess air quality and climate impacts. Few such in-situ measurements exist but are essential because the theoretical mechanisms dealing with the physico-chemical processes in the atmosphere are often better known than the detailed composition of the volcanic plume. The injection altitudes of volcanic emissions can vary significantly during an eruption, resulting in compositionally distinct plumes at different altitudes. In future, we aim to undertake comparison of the measurements made far downwind of the Holuhraun eruption source (several tens of km), as well as inter-compare the Holuhraun volcanic aerosol to that of other volcanoes measured using the LOAC either by balloon-based or ground-based sampling (as we have recently undertaken at Mt Etna), as well as remote sensing methods.

Acknowledgements

The LOAC team of the LPC2E/CNRS warmly thank all the persons from Icelandic Meteorological Office (IMO) and the University of Reykjavik for the support during this field campaign, the Cambridge scientist teams who have accepted our presence in their field campaign.

We acknowledge the ECMWF Archive product and Metview platform that enabled calculation of the backward trajectories. We also acknowledge the Icelandic team from IMO that produced the HARMONIE outputs, especially Bolli Pálmason.

This work is supported by the LABEX VOLTAIRE (ANR-10-LABX-100-01) from University of Orléans.

EC and RGG were supported by the NERC Centre for Observation and Modelling of Earthquakes, Volcanoes, and Tectonics (COMET) and from NERC grants NE/1015592/1 and NE/J023310/1.

AS was supported by an Academic Research Fellowship from the School of Earth and Environment at the University of Leeds, and EI and AS received NERC funding (NE/M021130/1).

Appendix A. Supplementary material

Supplementary material related to this article can be found online at http://dx.doi.org/10.1016/j.epsl.2016.08.027.

References

Barsotti, S., Neri, A., Scire, J.S., 2008. The VOL-CALPUFF model for atmospheric ash dispersal, 1: approach and physical formulation. J. Geophys. Res. 113, B03208. http://dx.doi.org/10.1029/2006JB004623.

Carboni, E., Grainger, R., Walker, J., Dudhia, A., Siddans, R., 2012. A new scheme for sulphur dioxide retrieval from IASI measurements: application to the Eyjafjallajökull eruption of April and May 2010. Atmos. Chem. Phys. 12, 11417–11434. http://dx.doi.org/10.5194/acp-12-11417-2012.

Carboni, E., Grainger, R.G., Mather, T.A., Pyle, D.M., Thomas, G.E., Siddans, R., Smith, A.J.A., Dudhia, A., Koukouli, M.E., Balis, D., 2016. The vertical distribution of volcanic SO_2 plumes measured by IASI. Atmos. Chem. Phys. 16, 4343–4367. http://dx.doi.org/10.5194/acp-16-4343-2016.

Galle, B., Johansson, M., Rivera, C., Zhang, Y., Kihlman, M., Kern, C., Lehmann, T., Platt, U., Arellano, S., Hidalgo, S., 2010. Network for Observation of Volcanic and Atmospheric Change (NOVAC)—a global network for volcanic gas monitoring: network layout and instrument description. J. Geophys. Res. 115, D05304. http://dx.doi.org/10.1029/2009JD011823.

Gíslason, S.R., Stefánsdóttir, G., Pfeffer, M.A., Barsotti, S., Jóhannsson, Th., Galeczka, I., Bali, E., Sigmarsson, O., Stefánsson, A., Keller, N.S., Sigurdsson, Á., Bergsson, B., Galle, B., Jacobo, V.C., Arellano, S., Aiuppa, A., Jónasdóttir, E.B., Eiríksdóttir, E.S., Jakobsson, S., Guðfinnsson, G.H., Alldórsson, S.A., Gunnarsson, H., Haddadi, B., Jónsdóttir, I., Thordarson, Th., Riishuus, M., Ögnadóttir, Th., Dürig, T., Pedersen, G.B.M., Höskuldsson, Á., Gudmundsson, M.T., 2015. Environmental pressure from

the 2014–15 eruption of Bárðarbunga volcano, Iceland. Geochem. Persp. Let. 1, 84–93.

Grattan, J., 1998. The distal impact of Icelandic volcanic gases and aerosols in Europe: a review of the 1783 Laki Fissure eruption and environmental vulnerability in the late 20th century. Geol. Soc. (Lond.) Spec. Publ. 15, 97–103. http://dx.doi.org/10.1144/GSL.ENG.1998.015.01.10.

Gudmundsson, M.T., Larsen, G., Höskuldsson, Á., Gylfason, Á.G., 2008. Volcanic hazards in Iceland. Jökull 58, 251–268.

Hammer, E., Gysel, M., Roberts, G.C., Elias, T., Hofer, J., Hoyle, C.R., Bukowiecki, N., Dupont, J.-C., Burnet, F., Baltensperger, U., Weingartner, E., 2014. Size-dependent particle activation properties in fog during the ParisFog 2012/13 field campaign. Atmos. Chem. Phys. 2014/05/15, 6.81.

Ilyinskaya, E., Martin, R.S., Oppenheimer, C., 2012. Aerosol formation in basaltic lava fountaining: Eyjafjallajökull volcano, Iceland. J. Geophys. Res., Atmos. 117, D00U27. http://dx.doi.org/10.1029/2011JD016811.

Jégou, F., Berthet, G., Brogniez, C., Renard, J.-B., François, P., Haywood, J.M., Jones, A., Bourgeois, Q., Lurton, T., Auriol, F., Godin-Beekmann, S., Guimbaud, C., Krysztofiak, G., Gaubicher, B., Chartier, M., Clarisse, L., Clerbaux, C., Balois, J.Y., Verwaerde, C., Daugeron, D., 2013. Stratospheric aerosols from the Sarychev volcano eruption in the 2009 Arctic summer. Atmos. Chem. Phys. 13, 6533–6552. http://dx.doi.org/10.5194/acp-13-6533-2013.

Kroll, J.H., Cross, E.S., Hunter, J.F., Pai, S., Wallace, L.M.M., Croteau, P.L., Jayne, J.T., Worsnop, D.R., Heald, C.L., Murphy, J.G., Frankel, S.L., 2015. Atmospheric evolution of sulfur emissions from Kīlauea: real-time measurements of oxidation, dilution, and neutralization within a volcanic plume. Environ. Sci. Technol. 49, 4129–4137.

Lurton, T., Renard, J.-B., Vignelles, D., Jeannot, M., Akiki, R., Mineau, J.-L., Tonnelier, T., 2014. Light scattering at small angles by atmospheric irregular particles: modelling and laboratory measurements. Atmos. Meas. Tech. 7, 931–939. http://dx.doi.org/10.5194/amt-7-931-2014.

Marenco, F., Johnson, B., Turnbull, K., Newman, S., Haywood, J., Webster, H., Ricketts, H., 2011. Airborne lidar observations of the 2010 Eyjafjallajökull volcanic ash plume. J. Geophys. Res., Atmos. 116, D00U05. http://dx.doi.org/10.1029/2011JD016396.

Martin, R.S., Mather, T.A., Pyle, D.M., 2006. High-temperature mixtures of magmatic and atmospheric gases. Geochem. Geophys. Geosyst. 7, Q04006. http://dx.doi.org/10.1029/2005GC001186.

Martucci, G., Ovadnevaite, J., Ceburnis, D., Berresheim, S., Varghese, S., Martin, D., Flanagan, R., O'Dowd, C.D., 2012. Impact of volcanic ash plume aerosol on cloud microphysics. Atmos. Environ. 48, 205–218.

McCormick, M.P., Thomason, L.W., Trepte, C.R., 1995. Atmospheric effects of the Mt Pinatubo eruption. Nature 373, 399–404. http://dx.doi.org/10.1038/373399a0.

McGonigle, A.J.S., Aiuppa, A., Giudice, G., Tamburello, G., Hodson, A.J., Gurrieri, S., 2008. Unmanned aerial vehicle measurements of volcanic carbon dioxide fluxes. Geophys. Res. Lett. 35, L06303. http://dx.doi.org/10.1029/2007GL032508.

Pieri, D., Diaz, J.A., Bland, G., Fladeland, M., Madrigal, Y., Corrales, E., Alegria, O., et al., 2013. In situ observations and sampling of volcanic emissions with NASA and UCR unmanned aircraft, including a case study at Turrialba Volcano, Costa Rica. Geol. Soc. (Lond.) Spec. Publ. 380, 321–352.

Renard, J.-B., Dulac, F., Berthet, G., Lurton, T., Vignelles, D., Jégou, F., Tonnelier, T., Jeannot, M., Couté, B., Akiki, R., Verdier, N., Mallet, M., Gensdarmes, F., Charpentier, P., Mesmin, S., Duverger, V., Dupont, J.-C., Elias, T., Crenn, V., Sciare, J., Zieger, P., Salter, M., Roberts, T., Giacomoni, J., Gobbi, M., Hamonou, E., Olafsson, H., Dagsson-Waldhauserova, P., Camy-Peyret, C., Mazel, C., Décamps, T., Piringer, M., Surcin, J., Daugeron, D., 2016. LOAC: a small aerosol optical counter/sizer for ground-based and balloon measurements of the size distribution and nature of atmospheric particles, part 1: principle of measurements and instrument evaluation. Atmos. Meas. Tech. 9, 1721–1742. http://dx.doi.org/10.5194/amt-9-1721-2016.

Roberts, T.J., Martin, R.S., Jourdain, L., 2014. Reactive bromine chemistry in Mount Etna's volcanic plume: the influence of total Br, high-temperature processing, aerosol loading and plume–air mixing. Atmos. Chem. Phys. 14 (20), 11201–11219.

Robock, A., 2000. Volcanic eruptions and climate. Rev. Geophys. 38, 191–219.

Rodgers, C.D., 2000. Inverse Methods for Atmospheric Sounding: Theory and Practice. World Scientific Publishing Co. Ltd.

Saunders, R., Matricardi, M., Brunel, P., 1999. An improved fast radiative transfer model for assimilation of satellite radiance observations. Q. J. R. Meteorol. Soc. 125, 1407–1425. http://dx.doi.org/10.1002/qj.1999.49712555615.

Schmidt, A., Carslaw, K.S., Mann, G.W., Rap, A., Pringle, K.J., Spracklen, D.V., Wilson, M., Forster, P.M., 2012. Importance of tropospheric volcanic aerosol for indirect radiative forcing of climate. Atmos. Chem. Phys. 12, 7321–7339. http://dx.doi.org/10.5194/acp-12-7321-2012.

Schmidt, A., Leadbetter, S., Theys, N., Carboni, E., Witham, C.S., Stevenson, J.A., Birch, C.E., Thordarson, T., Turnock, S., Barsotti, S., Delaney, L., Feng, W., Grainger, R.G., Hort, M.C., Höskuldsson, Á., Ialongo, I., Ilyinskaya, E., Jóhannsson, T., Kenny, P., Mather, T.A., Richards, N.A.D., Shepherd, J., 2015. Satellite detection, long-range transport, and air quality impacts of volcanic sulfur dioxide from the 2014–2015 flood lava eruption at Bárðarbunga (Iceland). J. Geophys. Res., Atmos. 120, 2015JD023638. http://dx.doi.org/10.1002/2015JD023638.

Schmidt, A., Ostro, B., Carslaw, K.S., Wilson, M., Thordarson, Th., Mann, G.W., Simmons, A.J., 2011. Excess mortality in Europe following a future Laki-style Icelandic eruption. Proc. Natl. Acad. Sci. USA 108 (38), 15710–15715. http://dx.doi.org/10.1073/pnas.1108569108.

Seity, Y., Brousseau, P., Malardel, S., Hello, G., Bénard, P., Bouttier, F., Lac, C., Masson, V., 2011. The AROME-France convective-scale operational model. Mon. Weather Rev. 139, 976–991. http://dx.doi.org/10.1175/2010MWR3425.1.

Shinohara, H., 2013. Composition of volcanic gases emitted during repeating Vulcanian eruption stage of Shinmoedake, Kirishima volcano, Japan. Earth Planets Space 65 (6), 667–675.

Solomon, S., Daniel, J.S., Neely, R.R., Vernier, J.-P., Dutton, E.G., Thomason, L.W., 2011. The persistently variable "background" stratospheric aerosol layer and global climate change. Science 333, 866–870. http://dx.doi.org/10.1126/science.1206027.

Spinetti, C., Barsotti, S., Neri, A., Buongiorno, M.F., Doumaz, F., Nannipieri, L., 2013. Investigation of the complex dynamics and structure of the 2010 Eyjafjallajökull volcanic ash cloud using multispectral images and numerical simulations. J. Geophys. Res., Atmos. 118, 4729–4747. http://dx.doi.org/10.1002/jgrd.50328.

Stohl, A., Hittenberger, M., Wotawa, G., 1998. Validation of the Lagrangian particle dispersion model FLEXPART against large-scale tracer experiment data. Atmos. Environ. 32, 4245–4264.

Taylor, S., Durand, M., Grattan, J., 2003. Illness and elevated human mortality in Europe coincident with the Laki Fissure eruption.

Thordarson, T., Self, S., 2003. Atmospheric and environmental effects of the 1783–1784 Laki eruption: a review and reassessment. J. Geophys. Res. 108 (D1), 4011.

Warner, J., 1969. The microstructure of cumulus cloud, part I: general features of the droplet spectrum. J. Atmos. Sci. 26 (2), 1049–1059. http://dx.doi.org/10.1175/1520-0469(1969)026<1049:TMOCCP>2.0.CO.

Witham, C.S., Oppenheimer, C., 2004. Mortality in England during the 1783–4 Laki Craters eruption. Bull. Volcanol. 67, 15–26. http://dx.doi.org/10.1007/s00445-004-0357-7.